SANS AND SAXS STUDY ON AQUEOUS MIXTURES OF FULLERENE-BASED STAR IONOMERS AND SODIUM DODECYL SULFATE

by

U. Jeng, W. -J. Liua, and T. -L. Lin
Department of Engineering and System Science
National Tsing Hua University
Hsinchu 30043 Taiwan
and
C. -S. Tsao
Division of Nuclear Fuel and Materials
Institute of Nuclear Energy Research
Lungtan 325 Taiwan
and
T. Canteenwala and L. Y. Chiang
Center for Condensed Matter Sciences
National Taiwan University
Taipei 106, Taiwan
and
L.P. Sung and C. C. Han
National Institute of Standards and Technology
Gaithersburg, MD 20899-8621 USA

NIST

National Institute of Standards and Technology
Technology Administration, U.S. Department of Commerce

SANS and SAXS study on aqueous mixtures of fullerene-based star ionomers and sodium dodecyl sulfate

U. Jeng[a], T.-L. Lin[a, *], W.-J. Liu[a], C.-S. Tsao[b], T. Canteenwala[c], L.Y. Chiang[c], L.P. Sung[d], C.C. Han[d]

[a] Department of Engineering and System Science, National Tsing Hua University, Hsinchu 30043, Taiwan
[b] Division of Nuclear Fuel and Materials, Institute of Nuclear Energy Research, Lungtan 325, Taiwan
[c] Center for Condensed Matter Sciences, National Taiwan University, Taipei 10617, Taiwan
[d] National Institute of Standards and Technology, Gaithersburg, MD 02899, USA

Abstract

Fullerene-based star ionomer $C_{60}[CO(CH_2)_5O(CH_2)_4SO_3Na]_6$ ($FC_{10}S$), with six sodium-dodecyl-sulfate-like arms randomly bonded on the fullerene, has been synthesized. This novel molecule has a high water solubility and a structural shape resembling the skeleton of a micelle of sodium dodecyl sulfate (SDS). We study aqueous mixtures of the C_{60}-based ionomers and SDS using small angle neutron scattering (SANS) and small angle X-ray scattering (SAXS). With a selected deuteration of SDS, we have identified the formation of complex aggregates of $FC_{10}S$ with SDS in the mixtures. The structural information of the complex aggregates is extracted from the SANS and SAXS data measured for the mixtures. On the average, the complex aggregates observed have a cylinder-like shape with a radius of 19 Å and a length of ≈ 100 Å for the sample mixtures containing 2.3 or 1.2 mM of $FC_{10}S$ and 6 mM of SDS. The mean aggregation numbers of $FC_{10}S$ and SDS in each complex aggregate are 15 and 11, respectively. © 2002 Elsevier Science B.V. All rights reserved.

Keywords: SANS; SAXS; Fullerene-derived ionomers; Aggregation structure

1. Introduction

Recently, we have synthesized fullerene-based ionomers $C_{60}[(CH_2)_4SO_3Na]_6$ (FC_4S) for potential biomedical applications such as free radical scavenging or antioxidant-action
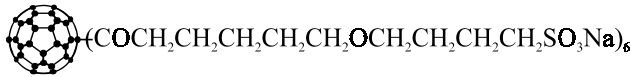

Fig. 1. Schematic view of a fullerene-based star ionomer $FC_{10}S$.

facilitating [1,2]. With the six sulfobutyl arms randomly bounded on the C_{60} cage, the star-like FC_4S has high water solubility. In our previous studies, using SANS and SAXS, we found that FC_4S formed globular aggregates of a nano-scale size in aqueous solutions [3,4]. In a continued study for the effect of arm-length on aggregation behaviors, the six sulfobutyl arms of FC_4S were extended to a length similar to SDS. The long-arm fullerene-based ionomers, $C_{60}[CO(CH_2)_5O(CH_2)_4SO_3Na]_6$ ($FC_{10}S$) were found to form rod-like aggregates in water solutions, with a much larger aggregation number (more than four folds) and stronger interparticle interactions than that for FC_4S [5].

Due to the constraint of the star-like morphology, both these C_{60}-ionomers seem to have an aggregation structure of "loose" hydrophobic-rich regions and a high water content for the aggregates. Such a structure is very different from the typical closely packed hydrophobic core structure for the linear type of surfactants. It will be interesting to know how the aggregation structure of loose hydrophobic regions for the star-like C_{60}-ionomers influences their interactions with surfactants, lipids, or polymers. Also, due to the unique physical characteristics of fullerenes and the star-like morphology, we expect that $FC_{10}S$ can lead to different microstructures from that formed by SDS in complex solutions. For instance, in mixtures of SDS and dodecyltrimethylammonium (DTAB) [6,7] the transformation of the rod-like micelles into vesicles or lamellar sheets may be suppressed when the linear SDS is replaced by the star-like $FC_{10}S$ (Fig. 1). In such cases, $FC_{10}S$ may be used to stabilize the micellar phase of the mixtures. It is also interesting to study the effect of $FC_{10}S$ in SDS-protein [8] or SDS-polymer systems [9,10], where bindings of surfactants to proteins or polymers have been observed. The surfactant-binding effect may have implications for applications of $FC_{10}S$ in biomedical systems, such as preventing formation of the toxic β-sheet structure of amyloid β-peptide that is responsible for Alzheimer's disease [11].

Here, we report a study of aqueous mixtures containing $FC_{10}S$ and SDS. In this system we ask whether star $FC_{10}S$ with SDS-like arms can absorb SDS and form compact core-shell structure similar to SDS micelles. In extracting the structural information of the mixed complex aggregates of C_{60}-ionomers and SDS we adapt SAXS and SANS with the contrast variation method [12,13] as described below.

2. Scattering model and contrast variation for SANS and SAXS

Small angle scattering (SAS) for particles of a monodisperse size in a colloidal solution can be modeled as [14]

$$I(Q) = I_0 \tilde{P}(Q) S(Q) . \tag{1}$$

In the above equation $\tilde{P}(Q)$ is the normalized form factor with $\tilde{P}(0)=1$, and $S(Q)$ the structure factor. The wave vector transfer $Q=4\pi\sin(\theta/2)/\lambda$ is defined by the scattering angle θ and the wavelength λ of the radiation quanta, whereas $I_0=n_p(\rho-\rho_w)^2V^2$ is the scattering amplitude with the number density n_p and the volume V for the particles. The scattering length density (SLD) for the particles and the solvent are denoted by ρ and ρ_w, respectively. For rod-like particles,

$$\tilde{P}(Q) = \int_0^1 \left| \frac{2J_1(v)}{v} \frac{\sin(w)}{w} \right|^2 d\mu \,. \tag{2}$$

The above form factor is averaged from the spatial orientations of right-circular cylinders of radius r and length L, with $v=Qr(1-\mu^2)^{1/2}$, $w=(1/2)QL\mu$, and the first order Bessel function J_1 [15,16].

For a cylindrical aggregate containing, respectively, N_i, N_w, and N_s numbers of C_{60}-based ionomers $FC_{10}S$, water, and SDS molecules, we can construct a scattering length density $\rho = (N_ib_i + N_wb_w + N_sb_s)/V$ for the complex aggregate, where $V=(N_iV_i+N_wV_w+N_sV_s)$. The symbols b_i, b_w, b_s and V_i, V_w, V_s denote, respectively, the scattering lengths and volumes for $FC_{10}S$, D_2O, and SDS [17]. We can now write I_0 in Eq. (1) as

$$I_0 = n_p[N_i(b_i - \rho_wV_i) + N_s(b_s - \rho_wV_s)]^2 \,. \tag{3}$$

From Eq. (3), we see that I_0 can be changed significantly when SDS molecules ($b_s = 16.0$ fm) in the aggregate are replaced by d-SDS ($b_s = 276.2$ fm) of a much higher scattering length, presuming that there are non-trivial SDS molecules in the aggregate ($N_s \neq 0$). Furthermore, the deuteration will not change the scattering profile, provided that SDS molecules distribute uniformly in the aggregate [17]. Here, we neglect the possible isotope effect on the structure of the aggregates, which seems safe when the system studied is not close to critical conditions for phase transitions [18,19]. An estimation for the scattering length density of $FC_{10}S$, SDS, d-SDS, and D_2O shows (see Fig. 2) that the SANS contrast for the complex aggregates in D_2O solutions is
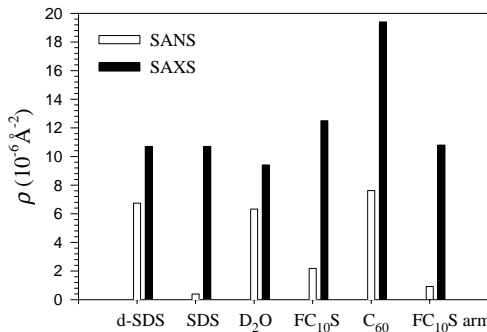

Fig. 2. SANS (empty bars) and SAXS (solid bars) scattering-length-density ρ for the related chemical groups. The volumes used in the calculations are 410 $Å^3$ for SDS, 2780 $Å^3$ for $FC_{10}S$, 377 $Å^3$ for an $FC_{10}S$ arm, and 524 $Å^3$ for C_{60}.

mainly contributed by the arms of $FC_{10}S$ and SDS of low ρ values, whereas the SAXS contrast for the same system is provided largely by the C_{60} of $FC_{10}S$, which has a much higher scattering length density than that for water or the arms of $FC_{10}S$.

3. Experiment

3.1. Synthesis

The synthesis route for the fullerene-based ionomers hexa(sulfobutoxypentylcarboxy)[60]-fullerene has been reported in Ref. [5]. Here we only brief the procedures. The sodium naphthalide reagent was allowed to react with C_{60} in toluene. Caprolactone was then added to the reaction mixture for the intermediate of hexa(hydroxypentylcarboxy)[60]fullerene sodium salt. The reaction of this sodium salt with 1,4-butane sultone was carried out to afford the product of hexa(sulfobutoxypentylcarboxy)[60]fullerene in 45% yield after purification.

3.2. Measurements

In preparing $FC_{10}S$/SDS mixtures, we kept the SDS concentration lower than the critical micelle concentration (CMC) for SDS, which is 8 mM [19], to avoid the complication due to the scattering contribution from pure SDS micelles. Under this condition, two contrast-variation systems with different $FC_{10}S$/SDS ratios were prepared. The first system included two D_2O mixtures of 2.33 mM of $FC_{10}S$ ionomers, respectively, with 6-mM SDS and 6-mM d-SDS added. For the second system, a lower $FC_{10}S$ concentration of 1.17 mM was used in another two D_2O solutions containing 6-mM SDS and 6-mM d-SDS, respectively.

Sample solutions were charged, individually, into quartz cells of a 5-mm path length for SANS measurements, which were conducted under a controlled temperature ($23 \pm 0.5°C$) on the 8-m SANS instrument at the National Institute of Standards and Technology (NIST). Pinholes of 2.5 and 1 cm diameters separated by 4.1 m were used to collimate the incident beam of a wavelength of 5 Å. The wavelength dispersion $(\Delta\lambda/\lambda)_{FWHM}$ of the beam is 25%. With the center of the two-dimensional detector shifted $6°$ away from the direct beam and a sample-to-detector distance of 3.6 m, the data measured covered a Q-range from 0.01 to 0.2 Å^{-1}. The transmissions measured for all sample solutions were all close to the 5-mm D_2O transmission 0.66. Data were corrected for sample transmission, background, and detector sensitivity, and normalized to an absolute scattering scale, scattering cross section per unit sample volume $I(Q)$, by comparison to the scattering from H_2O [20]. The uncertainty for the $I(Q)$ thus calibrated is estimated to be 5–10%.

SAXS measurements for the sample solutions contained in 1-mm-thick cells of Kapton windows were performed on the 8-m SAXS instrument at Tsing-Hua University, Hsinchu [21]. The incident beam, from an 18-kW rotating-anode X-ray source, was collimated by three pinholes of diameters 1.0, 1.0, and 2.0 mm, arranged in 3.1-m path length. With a beam wavelength of 1.54 Å and a sample-to-detector distance of

2.3 m, the SAXS instrument scanned the scattering intensity in a Q range from 0.02 to 0.22 Å^{-1}. Data were collected by a two-dimensional area detector, and corrected for sample transmission, background, and detector sensitivity, and normalized to an absolute scattering scale by comparison to the scattering from a secondary standard sample of lead stearate. The accuracy for SAXS $I(Q)$ thus calibrated is within ±10%.

4. Results and analysis

4.1. SANS and SAXS data

Fig. 3 shows the SANS data for the mixtures of 2.33-mM FC$_{10}$S with 6-mM SDS (squares) and 6-mM d-SDS (circles), respectively. The apparent difference in the intensities and the similarity in the scattering profiles highly suggest that the system contains complex aggregates of FC$_{10}$S with SDS, as explained in the previous section for the scattering characteristics of the complex aggregates. In addition, the profiles for the mixtures measured in most of the Q-region resemble that for the pure FC$_{10}$S solution of 2.33 mM (diamonds), indicating that the complex aggregates have a cylinder-like structure similar to that for pure FC$_{10}$S aggregates observed in a previous study [5].

Since d-SDS has a scattering length density close to that for D$_2$O (see Fig. 2), its monomers or micelles in D$_2$O solutions are virtually invisible to neutrons. Therefore, most of the data measured in an absolute intensity scale for the FC$_{10}$S/d-SDS mixture
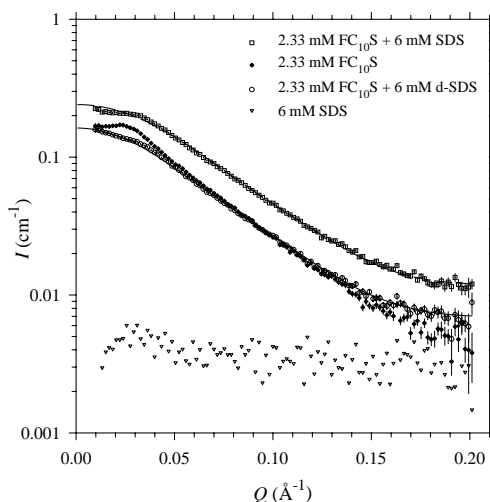

Fig. 3. SANS data for the two sample mixtures of 2.33-mM FC$_{10}$S containing 6-mM SDS (squares) and 6-mM d-SDS (circles), respectively. The two sets of contrast data are fitted (dashed and solid curves) jointly with the SAXS data (see Fig. 4) by a rod-like particle model with a hard sphere interaction. Also shown are the SANS data for a pure FC$_{10}$S solution of 2.33 mM (diamonds) and the SANS data for a pure SDS solution of 6 mM (triangles).
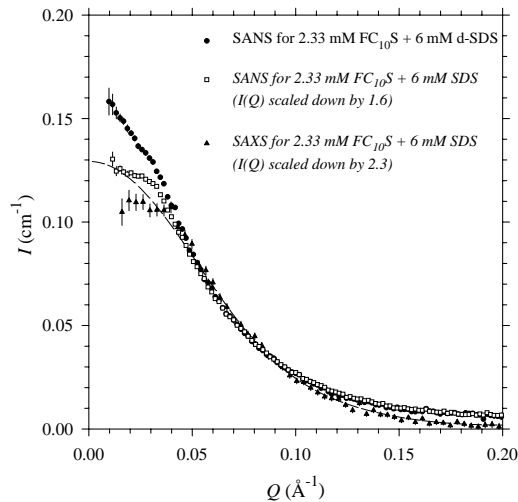
Fig. 4. The SANS data (squares) and SAXS data (triangles) for the sample mixtures of 2.33-mM $FC_{10}S$/6-mM SDS are scaled down by 1.6 and 2.3, respectively, to superimpose the SANS data (circles) for the $FC_{10}S$/d-SDS mixture. The SAXS data are fitted (dashed curve) together with the two sets of SANS data by a rod-like model.

are nearly the same as that for the pure $FC_{10}S$ solution. For a closer look at the low-Q region ($Q \lesssim 0.03 \text{ Å}^{-1}$), the profile for the $FC_{10}S$/d-SDS mixture departs from that for the pure $FC_{10}S$ solution. This deviation should result from (1) a smaller rod length for the $FC_{10}S$/SDS aggregates, and (2) smaller interactions between the complex aggregates (corresponding to a less obvious scattering shoulder) for the mixing system, as compared with the pure $FC_{10}S$ system [17]. The smaller interaction observed for the complex aggregates may be due to a charge-screening effect induced by the free ionic d-SDS monomers in the solution [19]. As in common ionic micellar solutions of high concentrations, the charge screening effect is often achieved by adding salt into the solutions [22,23].

In Fig. 3, we also show the SANS result (triangles) for a pure SDS solution of 6 mM in D_2O. The relatively flat SANS spectrum confirms that the scattering contribution from SDS micelles or monomers is negligible at this surfactant concentration, since 6 mM is lower than the CMC of SDS.

After a proper scaling for superimposing, we observe that the SANS profile for the $FC_{10}S$/SDS mixture deviates downward slightly from that for the $FC_{10}S$/d-SDS mixture in the small-Q region as shown in Fig. 4. Since the structure factor of a system does not change with the selected deuteration of SDS in the system [17], this discrepancy should result solely from a difference in the form factor. In fact, the radius of gyration R_g may change with the contrast variation used, when the deuterated component is not uniformly distributed in an aggregate [17]. The small discrepancy observed, therefore, indicates that the SDS molecules distribute in a slightly inward region of the complex aggregate. This leads to a smaller R_g for $FC_{10}S$/SDS aggregates in D_2O, as compared
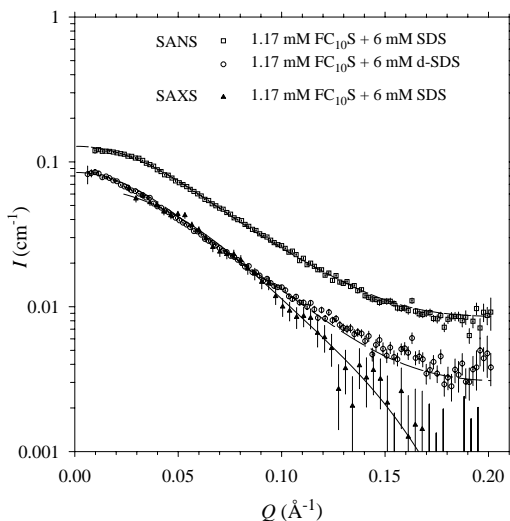
Fig. 5. The two sets of SANS data and one set of SAXS data for the sample mixtures of 1.17-mM $FC_{10}S$ are fitted jointly (dashed and solid curves) with the same model used for the first system.

to the R_g for $FC_{10}S$/d-SDS aggregates in D_2O. (Numerical values for R_g will be given below.)

For the SAXS result, since the X-ray scattering length densities for SDS and $FC_{10}S$ arms are both close to that for water, the SAXS profiles measured for $FC_{10}S$/SDS mixtures are dominated by the C_{60} cages of $FC_{10}S$ (see Fig. 2). After scaling down by a factor of 2.3, the SAXS profile measured for the mixture of 2.33-mM $FC_{10}S$ and 6-mM SDS (triangles in Fig. 4) can overlap approximately the SANS profiles for the same solution. In the low-Q region, the SAXS profile deviates downwards from the SANS profiles. These SAXS features indicate that the C_{60} cages in the aggregate distribute in a cylinder-like region of similar radius but smaller length, in comparison with the distribution of $FC_{10}S$ arms observed from the SANS data. In other words, the $FC_{10}S$ arms extend outwards slightly more than the C_{60} cages do, especially in the longitudinal direction of the aggregate.

For the second system of a lower $FC_{10}S$ concentration of 1.17 mM, Fig. 5 shows the SAS data for the two sample solutions, respectively, treated with 6-mM SDS (squares and triangles) and 6-mM d-SDS (circles). These three scattering profiles are similar to those for the first system. Indeed, after normalizing to the $FC_{10}S$ concentration, the three SAS profiles can overlap well the corresponding profiles of the first system. Such a result implies that (1) the structure of the complex aggregates does not change with the $FC_{10}S$ concentrations studied, and (2) the scattering intensity is essentially linearly proportional to the $FC_{10}S$ concentration. The latter suggests that nearly all C_{60}-based star ionomers in the mixtures form complex aggregates [3], namely, $n_p \approx C/N_i$, where C is the concentration of $FC_{10}S$ and N_i the average number of $FC_{10}S$ per aggregate.

4.2. Model fitting

In extracting the structural information for the $FC_{10}S$/SDS aggregates, we fit jointly the three sets of SAS data for the solutions of 2.33-mM $FC_{10}S$ using a rod-like particle model [4,18]. Adapting $V_s = 410$ Å^3 from Cabane et al. [24] and using $n_p = C/N_i$, we have independent fitting parameters N_i, V_i, and N_s (see Eqs. (2) and (3)). In principle, the three parameters N_i, V_i, and N_s can be determined uniquely by the absolute scattering intensities of the three sets of contrast data. Since the interparticle interaction is small, we may approximate $S(Q)$ for the system by a structure factor generated from the Percus–Yevick hard sphere model [25], with a volume fraction $\eta = n_p V$ and an effective sphere diameter σ from $V = \pi r^2 L = 4/3\pi(\sigma/2)^3$. This approximation is reasonable when the L/σ ratio is smaller than about 2 [17]. For larger values, we use a more elaborated form for σ as described in Ref. [5]. Note, the common $S(Q)$ used for the three sets of SAS data adds no additional parameters to the fitting process. We also take into account the smearing effect of $I(Q)$ due to the divergence and the wavelength dispersion of the beam for the SANS and SAXS data, respectively, in a non-linear fitting process for a least χ^2 contributed by the three sets of data.

The fitting result (dashed and solid curves in Fig. 3 for the SANS data, dashed curve in Fig. 4 for the SAXS data) demonstrates that all three sets of data can be described simultaneously well by cylindrical-like particles having compositions of $N_i = 15 \pm 1$ and $N_s = 11 \pm 1$, with $V_i = 2420 \pm 50$ Å^3. The dry volume V_i obtained for $FC_{10}S$ is close to 2780 Å^3 estimated from a C_{60}-cage and six arms of $FC_{10}S$. The R_g values for the complex aggregates can be obtained from the best-fitted r and L values summarized in Table 1 using $R_g = (r^2/2 + L^2/12)^{1/2}$ [15]. In fact, the R_g values are more meaningful than the L values that are determined using the approximation of a homogeneous aggregate in the model. They are 32.9 and 28.6 Å, respectively, for the $FC_{10}S$/d-SDS and $FC_{10}S$/SDS aggregates observed by SANS, and 24.3 Å for the

Table 1
Summary of the fitting results for the SAS data[a]

	$FC_{10}S$ (mM)	SDS (mM)	R_g (Å)	r (Å)	L (Å)[b]
SANS	2.33	6.0 (d-SDS)	32.9	19.5 ± 0.6	103 ± 6
	2.33	6.0 (SDS)	28.9	19.5 ± 0.6	88 ± 4
SAXS	2.33	6.0 (SDS)	24.8	19.2 ± 1.5	72 ± 10
SANS	1.17	6.0 (d-SDS)	32.9	19.5	103
	1.17	6.0 (SDS)	28.9	19.5	88
SAXS	1.17	6.0 (SDS)	24.8	19.2	72

[a]The SAS data are fitted using a rod-like particle model with a hard sphere interaction. The radius of gyration R_g is derived from the radius r and length L fitted for the cylinder-like aggregates. For the mixtures of 2.23-mM $FC_{10}S$, the volume fraction $\eta = 0.012$ and $S(0) = 0.91$, whereas $\eta = 0.006$ and $S(0) = 0.95$ for the mixtures of 1.17-mM $FC_{10}S$. The aggregation numbers obtained for the complex aggregates in both mixtures are $N_i = 15 \pm 1$ for $FC_{10}S$ and $N_s = 11 \pm 1$ for SDS (or d-SDS), with the dry volume $V_i = 2420 \pm 50$ Å^3 for $FC_{10}S$. Note, an ellipsoidal model, with a semi-major axis of ≈ 70 Å and a semi-minor axis of ≈ 20 Å, can fit the data as well with the same N_i, N_s, and V_i values as that obtained from the rod-like model.

[b]The length of a stretched $FC_{10}S$ arm is about 15 Å.

$FC_{10}S/SDS$ aggregates observed by SAXS. These R_g values relate subsequently to the distribution of $FC_{10}S$ arms, SDS molecules, and the C_{60}-cages of $FC_{10}S$ in the complex aggregate, as discussed previously. Again, the result indicates that the fullerenes of the star $FC_{10}S$ distribute more inwards in the complex structure. While the SDS adsorbed fills mainly in the center region of the rod-like aggregates, but not the ends of the aggregate. Compared to pure $FC_{10}S$ aggregates, the radius for the complex aggregates obtained (see Table 1) is nearly the same, whereas the length is significantly smaller ($\sim$50%). Using $V = \pi r^2 L = N_i V_i + N_w V_w + N_s V_s$ with $r = 19.5$ Å, $L = 103$ Å, and $V_w = 30.3$ Å^3 [22] we can deduce a water content $N_w = 2700 \pm 200$ for the complex aggregate. Such a water content occupies roughly 60% of the aggregate volume.

In Fig. 5, we show that the three sets of SAS for the second system of 1.17-mM $FC_{10}S$ can also be fitted (dashed and solid curves) satisfactorily using exactly the same structural parameters (see Table 1) as that for the first system. The result implies that the critical concentration for forming the complex aggregates of $FC_{10}S/SDS$ is much lower than the $FC_{10}S$ concentrations studied.

5. Discussion and conclusions

Using SAXS and SANS with the contrast variation method, we have found that C_{60}-based star ionomers $FC_{10}S$ form complex aggregates with SDS in water solutions. In comparison with pure $FC_{10}S$ aggregates [5], the aggregation number of $FC_{10}S$ in $FC_{10}S/SDS$ mixtures is significantly lowered ($\sim$50%) due to the intervening of SDS molecules. The ratio N_s/N_i between the deduced aggregation numbers of SDS and $FC_{10}S$ is $\approx$0.7, which can be regarded as a mean SDS-absorption efficiency for $FC_{10}S$. Furthermore, the higher SDS-excess concentration in the second system of a lower $FC_{10}S$ concentration does not lead to a higher SDS-absorption efficiency. It seems that the SDS-absorption efficiency for $FC_{10}S$ is insensitive to the SDS concentrations in the mixtures, when the SDS concentrations are lower than their CMC. From the composition obtained for the complex aggregates, we deduce the free SDS in the 2.33 and 1.17 mM $FC_{10}S/SDS$ systems to be about 4.4 and 5.2 mM, respectively.

The SDS-absorption efficiency observed for $FC_{10}S$ is low, considering that each star ionomer $FC_{10}S$ has plenty of space in between the six SDS-like arms ready for SDS to settle in. For a comparison, the aggregation number for pure SDS micelles is > 60 [25]. Structurally speaking, the feature of loose hydrophobic regions for the $FC_{10}S/SDS$ complex aggregates, in comparison with the compact hydrophobic core for pure SDS micelles, suggests that the affinity of SDS to $FC_{10}S$ may not compete with the affinity between $FC_{10}S$ themselves. As a consequence, SDS molecules prefer not to park their aliphatic tails in the roomy core-near region of $FC_{10}S$ of a hydrophobic attribute, for a compact core-shell structure that we have anticipated.

The mechanism for forming the $FC_{10}S/SDS$ aggregates of small amount of SDS molecules may be explained by the existence of arm-rich regions in the complex aggregates. These arm-rich regions, presumably, are formed through the interactions between the aliphatic parts of the $FC_{10}S$ arms. For absorbing SDS monomers in a mixture of an SDS concentration lower than the CMC for SDS, the arm-rich sites must

provide a lower interfacial energy for the free SDS monomers to compensate the entropy loss of the system due to absorption. Following the argument, the SDS-absorption efficiency for $FC_{10}S$ is limited by the arm-rich sites available in the complex aggregates. Estimated from the composition for the complex aggregates obtained, each absorbed SDS associates averagely with 8 SDS-like arms from several $FC_{10}S$ in a complex aggregate. This number of arms should be sufficient for packing (trapping) an SDS monomer. From the above discussion, a higher SDS-absorption efficiency may be achieved by C_{60}-based star ionomers of more than six SDS-like arms, since more arms anchored on a C_{60} cage will increase the density of the arm-rich sites. The same goal may also be reached by lowering the system's entropy influence by lowering temperature.

Acknowledgements

References

[1] Y.L. Lai, W.-Y. Chiou, F.J. Lu, L.Y. Chiang, J. Pharmacol. 126 (1999) 778.
[2] S.S. Huang, Y.H. Chen, L.Y. Chiang, M.C. Tsai, Fullerenes Sci. Technol. 7 (4) (1999) 551.
[3] U. Jeng, T.-L. Lin, C.-S. Tsao, C.-H. Lee, L.Y. Wang, L.Y. Chiang, C.C. Han, J. Phys. Chem. B 103 (1999) 1059.
[4] C.-S. Tsao, T.-L. Lin, U. Jeng, J. Phys. Chem. Solids 60 (1999) 1351.
[5] W.-J. Liu, U. Jeng, T.-L. Lin, T. Canteenwala. L.Y. Chiang, Fullerenes Sci. Technol. 9 (2) (2001) 131.
[6] K.L. Herrington, E.W. Kaler, D.D. Miller, J.A. Zasadzinski, S. Chiruvolu, J. Phys. Chem. 97 (1993) 13 792.
[7] M. Bergström, J.S. Pedersen, Langmuir 14 (1998) 3754.
[8] S.-H. Chen, J. Teixeira, Phys. Rev. Lett. 57 (1986) 2583.
[9] J.-H. Kim, M.M. Domach, R.D. Tilton, J. Phys. Chem. 103 (1999) 10 582.
[10] B. Cabane, R. Duplessix, J. Phys. 48 (1987) 651.
[11] K.J. Marcinowski, H. Shao, E.L. Clancy, M.G. Zagorski, J. Am. Chem. Soc. 120 (1998) 11 082.
[12] J. Penfold, E. Staples, I. Tucker, Adv. Colloid Interface Sci. 68 (1996) 31.
[13] I.P. Purcell, J.R. Lu, R.K. Thomas, A.M. Howe, J. Penfold, Langmuir 14 (1998) 1637.
[14] T.-L. Lin, Physica B 180&181 (1992) 505.
[15] L.A. Feigin, D.I. Svergun, Structure Analysis by Small-Angle X-ray and Neutron Scattering, Plenum, New York, 1987, p. 69.
[16] S.H. Chen, Ann. Rev. Phys. Chem. 37 (1986) 351.
[17] S.-H. Chen, T.-L. Lin, in: K. Sköld, D.L. Price (Eds.), Methods of Experimental Physics—Neutron Scattering in Condensed Matter Research, Vol. 23B, Academic Press, New York, 1987 (Chapter 16).
[18] T. Zemb, P.J. Charpin, Physique 46 (1985) 249.
[19] B. Cabane, R.J. Duplessix, Physique 43 (1982) 1529.
[20] C.J. Glinka, J.G. Barker, B. Hammouda, S. Krueger, J.J. Moyer, W.J. Orts, J. Appl. Crystallogr. 31 (1998) 430.
[21] K. Linliu, S.-A. Chen, T.L. Yu, T.-L. Lin, C.-H. Lee, J.-J. Kai, S.-L. Chang, J.S. Lin, J. Polym. Res. 2 (1995) 63.

[22] Y.C. Liu, C.Y. Ku, P. LoNostro, S.-H. Chen, Phys. Rev. E 51 (1995) 4598.
[23] J.B. Hayter, J. Penfold, J. Chem. Soc. Faraday Trans. I 77 (1981) 1851.
[24] B. Cabane, R. Duplessix, T. Zemb, J. Phys. 46 (1985) 2161.
[25] I. Krakovsky, Z. Bubenikova, H. Urakawa, K. Kajiwara, Polymer 38 (1997) 3637.